

Plasmaron excitation and band renormalization in a two-dimensional electron gas

Paul von Allmen*

IBM Research Division, Zurich Research Laboratory, 8803 Rüschlikon, Switzerland

(Received 18 November 1991)

The structure of a plasmaron excitation is described for a two-dimensional electron gas at $T=0$ K. It is shown to lead to a staircaselike density of states with three steps. The band renormalization is then calculated by taking the imaginary part of the self-energy fully into account. The renormalization of the chemical potential is shown to be smaller than that of the edge of the density of states. The quasiparticle energy dispersion is strongly nonparabolic but the renormalization of the effective mass at the Fermi surface is found to be well approximated by the widely used lowest-order approximation.

I. INTRODUCTION

The plasmaron excitation was identified by Lundquist for a three-dimensional electron gas.¹ He showed that, aside from the usual quasiparticle peak, the spectral function presents a low-energy peak resulting from the resonant plasmon-hole coupling. He termed this additional peak *plasmaron* excitation. In a three-dimensional electron gas, plasmaron excitation leads to a satellite peak below the edge of the one-particle density of states (DOS). This structure gives a possible explanation for the low-energy tail observed in soft-x-ray emission spectra for light metallic elements.² It was also shown that the plasmaron excitation makes an important contribution to the cohesive energy of metals.²

The two-dimensional (2D) electron gas has been studied intensively in the past two decades. Several authors have calculated the self-energy corrections to the subband energy of electrons confined in semiconductor heterojunctions and quantum wells. Most of them used the standard random-phase approximation (RPA) with the charge-density fluctuations approximated by a single plasmon pole.³⁻⁵ Full RPA calculations have also been reported^{6,7} and local-field corrections have been considered in order to improve the evaluation of the effective mass and the Landé factor.⁸

For the evaluation of the band renormalization, the following assumptions are often made.

(i) In all the papers cited above, it is assumed that the band renormalization is given by the quasiparticle energy calculated by neglecting the effect of the imaginary part of the self-energy. Reference 9 takes this effect into account but only to a certain extent.

(ii) Most of these recent calculations use the zeroth-order approximation when evaluating the quasiparticle energy. This approximation consists of taking the self-energy at the noninteracting electron energy when solving the Dyson equation. Reference 3 already discussed this point in connection with the renormalization of the effective mass. Arguments have been given against and in support of the solution of the full Dyson equation.¹⁰

(iii) Many authors assume that the band shifts rigidly and hence that the shift of the chemical potential is equal to that of the edge of the DOS.

(iv) Finally, the band renormalization is usually reported to be a function of the density of the noninteracting electron gas. This makes the comparison with measurements difficult since only the density of the interacting electron gas is experimentally available.

In this work, I attempt to avoid these additional approximations. The spectral function for the 2D electron gas is calculated using the full RPA. The structure of the 2D plasmaron is thereby obtained and the density of states computed. This allows the electron density to be evaluated for a given chemical potential, fully including the real and imaginary parts of the self-energy. The renormalization of the energy band is then described by studying the shift of the chemical potential and of the edge of the DOS separately.

The main contributions of this work are (i) the description of the 2D plasmaron excitation, and (ii) a precise evaluation of the renormalization of the 2D energy band and a discussion of the rigid shift approximation.

The paper is organized as follows. Section II is a theoretical introduction. Section III describes the structure of the self-energy, the spectral function, and the corresponding DOS, and states the substantial differences from the 3D case. The last section discusses the shift of the chemical potential and of the edge of the DOS as well as the renormalization of the effective mass at the Fermi surface.

In a subsequent paper, I shall discuss the effects of the plasmaron excitation on the line shape of the intersubband absorption spectra in a confined electron gas.

II. THEORY

The spectral function $A(k, E)$ is related to the retarded self-energy $S(k, E)$ by the following expression:¹¹

$$A(k, E) = \frac{-2S_I(k, E)}{[E - \xi(k) - S_R(k, E)]^2 + [S_I(k, E)]^2}. \quad (1)$$

The kinetic energy of the noninteracting electron, with mass m , measured from the chemical potential μ is given by $\xi(k) = (\hbar^2/k^2/2m) - \mu$. The real (S_R) and imaginary (S_I) parts of the self-energy are obtained from the standard RPA expression. After the frequency summation,

we have the following equation:¹⁰

$$S(k, \omega) = -\frac{1}{(2\pi)^2} \int d^2q v_q n_F[\xi(\mathbf{k}+\mathbf{q})] \\ + \frac{1}{(2\pi)^2} \int d^2q v_q \int \frac{dE}{2\pi} C(q, E) \\ \times \frac{n_F[\xi(\mathbf{k}+\mathbf{q})] + n_B(E)}{E - \xi(\mathbf{k}+\mathbf{q}) + \omega + i\delta} . \quad (2)$$

The first term is the unscreened exchange contribution and the second one the correlation term. The charge-density fluctuations are described by $C(q, E) = -2 \operatorname{Im}[1 - v_q P^{(1)}(q, E)]^{-1}$, where $P^{(1)}(q, E)$ is the single bubble retarded polarization function whose analytical expression at $T=0$ K is well known for a 2D electron gas.¹² The 2D Fourier transform of the Coulomb potential is $v_q = e^2/2\epsilon q$ in mks units, where ϵ is the background static dielectric constant. The Fermi and Bose distribution functions are n_F and n_B .

The DOS is the sum over the momentum of the spectral function:

$$g(E) = \frac{2}{(2\pi)^2} \int d^2k \frac{A(k, E)}{2\pi} . \quad (3)$$

The charge density is the integral of the DOS weighted by the Fermi distribution function:

$$n_S = \int dE g(E) n_F(E) . \quad (4)$$

The corresponding chemical potential for a noninteracting electron gas is $\mu^{(0)} = \hbar^2 n_S \pi / m$ and the resulting renormalization of the chemical potential is $\Delta^{(\mu)} = \mu - \mu^{(0)}$. With this procedure, the variation of the shape of the DOS due to the electron-electron interaction and in particular the contribution of the imaginary part of the self-energy is fully included.

The shift of the edge of the DOS is determined by the position of the low-energy peak of the spectral function at $k=0, E^{(\text{QP})}(0)$. It is given by the solution of the following equation:

$$E - \xi(k) - S_R(k, E) = 0 . \quad (5)$$

The shift of the edge of the DOS is then $\Delta^{(\text{DOS})} = E^{(\text{QP})}(0) + \mu$.

In the literature, the band renormalization is computed in a different way. The charge density n_S is given and, using Luttinger's result that the Fermi momentum $k_F = \sqrt{2\pi n_S}$ is the same in an interacting and in a noninteracting electron gas,¹³ the chemical potential μ is given by the solution of (5) at $k=k_F$ in the lowest-order approximation,¹⁴ i.e.,

$$\mu = \mu^{(0)} + S_R^{(0)}(k_F, 0) . \quad (6)$$

As seen in (2), the chemical potential μ appears explicitly in the expression for the self-energy. In (6), however, S_R is computed by approximating μ to the chemical potential of the noninteracting electron gas, $\mu^{(0)}$,³ indicated by the superscript (0) in (6).

III. THE 2D PLASMARON

In this section I discuss the structure of the self-energy and of the spectral function as obtained from (2) and (1), respectively. Figure 1 displays these functions at $T=0$ K for a given chemical potential $\mu = 14$ meV and for various values of the momentum k . The electron effective mass is $m = 0.07m_0$ and the background relative dielectric constant is $\epsilon_r = 12$. These numbers are close to those used for an electron gas confined in a GaAs/Al_xGa_{1-x}As heterojunction.

Two values of k are important in this system. One is the Fermi momentum of the noninteracting electron gas, $k_0 = [(2m/\hbar^2)\mu]^{1/2}$. The other is the Fermi momentum of the interacting electron gas k_F at which the momentum distribution has a discontinuity.¹¹ The curves in Fig. 1 are given for these momenta and for values below and above them.

The imaginary part of the self-energy will now be discussed and its structure elucidated by considering the scattering events in the electron gas. A striking property is that $S_I(k, E)$ is small in a given energy region around the Fermi surface ($E=0$), the extension of which varies with k . I shall first discuss this point.

As noted by Lundquist,¹ the plasmon-pole contribution to the correlation term of the self-energy is similar to the self-energy for the polaron problem in a degenerate semiconductor.¹⁵ From there it can be deduced that this contribution must be zero in a region around the Fermi surface, where the electron or hole excitations cannot scatter to the Fermi surface by emitting a plasmon. For a 3D electron gas, the size of this region is almost the same for all momenta because the plasmon dispersion is almost flat at long wavelengths. For a 2D electron gas, the plasmon dispersion behaves like \sqrt{q} at long wavelengths, and therefore the momentum conservation during the electron-plasmon scattering implies that the size of the region is different for each momentum.

We now determine the boundaries of this region from the properties of the electron-plasmon scattering.

Figure 2 shows the plasmon energy dispersion and the energy $[\xi(q) - E]$ that is exchanged during the electron-plasmon scattering in a 2D electron gas at $k=0$. The shaded areas indicate the regions where the statistical factor ($n_F + n_B$) in (2) is nonzero at $T=0$ K. The meaning of this statistical factor is that only scattering events where a plasmon is emitted are allowed at $T=0$ K. The scattering events are given by the intersections of the plasmon and the electron dispersion curves. They contribute to S_I only if the intersections are in a shaded area. The upper half-plane ($E < 0$) is for the plasmon-hole scattering and the lower half-plane ($E > 0$) for the plasmon-electron scattering.

Figure 2 permits us to find the boundaries of the region where the plasmon-pole contribution to S_I is zero for $k=0$. For $k > 0$, the situation is somewhat more complicated because of the summation over the angle between \mathbf{k} and the plasmon momentum \mathbf{q} . It can be shown that the boundaries are given by the following expressions:

$$\xi(k) \leq E \leq \omega_p(k_0 - k) \quad \text{for } k < k_0 , \\ -\omega_p(k - k_0) \leq E \leq \xi(k) \quad \text{for } k > k_0 . \quad (7)$$

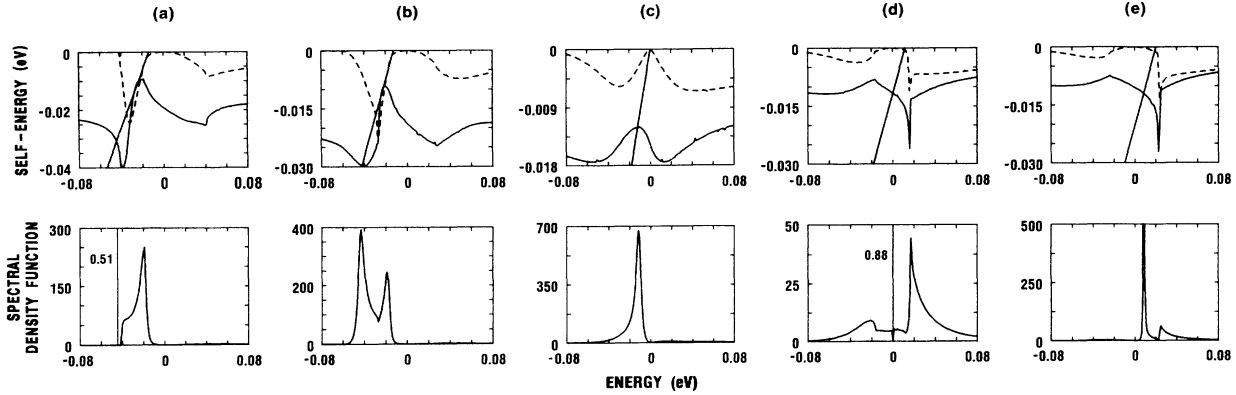


FIG. 1. Real (solid line) and imaginary (dashed line) part of the self-energy and spectral function for a 2D electron gas at $T=0$ K, for a chemical potential $\mu=13.7$ meV; (a) $k=0$, (b) $k=0.005 \text{ \AA}^{-1}$, (c) $k=k_0=0.016 \text{ \AA}^{-1}$, (d) $k=k_F=0.022 \text{ \AA}^{-1}$, and (e) $k=0.025 \text{ \AA}^{-1}$.

We note that for $k=k_0$ the domain reduces to a single point $E=0$, and that its size grows when k is larger or smaller than k_0 . Figure 1 displays this typical behavior.

S_I is not exactly zero in the region defined above because the electron-hole scattering, which is not ruled by the same constraints as the electron-plasmon scattering, also contributes to the charge-density fluctuations and hence to S_I .

The second important observation about the structure of S_I is that it presents a strong resonance or even a divergence situated below (above) the Fermi surface ($E=0$) for k below (above) k_0 . This peak is associated with a resonance in the joint density of states for the electron-plasmon scattering, which occurs when the electron and the plasmon energy dispersion curves are tangent. The resonance is at $E < 0$ (> 0) if the dispersion curves are tangent in the upper (lower) half-plane.

We now come to the discussion about the structure of the spectral function. Since the retarded self-energy is a causal function, its real and imaginary parts are related

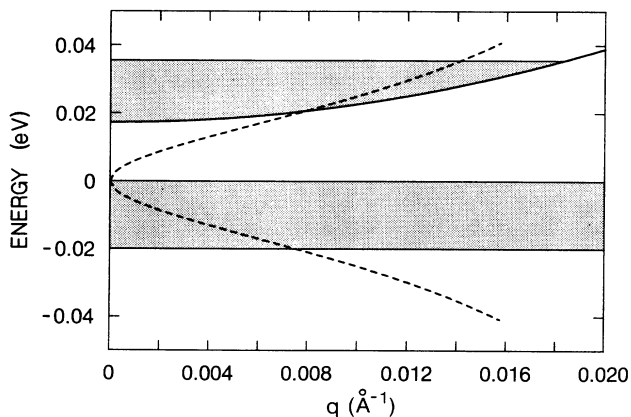


FIG. 2. Electron (solid line) and plasmon (dashed line) energy dispersion for a 2D electron gas. The initial energy in the electron-plasmon scattering ω is subtracted from the electron energy. The shaded areas indicate the regions where the scattered state is allowed to be at $T=0$ K.

by a Kramers-Kronig relation¹¹ and hence the real part presents a strong oscillation associated with the strong resonance in the imaginary part. As noted by Lundquist,¹ this implies that the spectral function has more than one peak. From the previous section, we know that the position of the peaks are given by the solutions of (5). These solutions are the quasiparticle energies whose damping is given by the imaginary part of the self-energy at that energy. Graphically, the solutions of (5) are given by the intersections of straight lines with the S_R curves (see Fig. 1).

At low k , there are three intersections. The low-energy intersection produces a peak in the spectral function that reduces to a δ function if the corresponding damping is zero (see first graph in Fig. 1). The number beside the δ function indicates its spectral weight. Lundquist called this peak a *plasmaron*.¹ It exists because there is a strong oscillation in S_R due to the strong resonance in S_I for $E < 0$. Therefore we can say that the plasmaron peak is caused by the resonant plasmon-hole coupling. The other two intersections in Fig. 1 produce a single broad peak because the corresponding damping is large. This peak corresponds to the usual dressed quasiparticle.² At higher k , the plasmaron peak broadens and merges with the high-energy peak at around $k=0.01 \text{ \AA}^{-1}$. Above $k \approx 0.01 \text{ \AA}^{-1}$ there is only one solution to (5), and the second peak in the spectral function is due to the strong resonance in S_I for $E > 0$. At $k=k_F$, most of the spectral weight is in the δ function centered at the Fermi surface ($E=0$), as expected from the Fermi liquid theory of Landau discussed in Ref. 16. We know that the integral of the spectral function over the entire energy range is equal to 1.¹¹ The curves in Fig. 1 fulfill this sum rule within less than 1%. This gives an indication of the numerical accuracy of the calculation.¹

The behavior of the spectral function described above is very similar to that found in the 3D case in Ref. 1. An essential difference is that in 3D the plasmaron peak disappears around $k=k_F$, whereas in 2D it merges with the other peak. To illustrate this fact, Fig. 3 displays the dispersion of the solutions to (5) and the corresponding damping. The low-energy solution at $k=0$ (plasmaron)

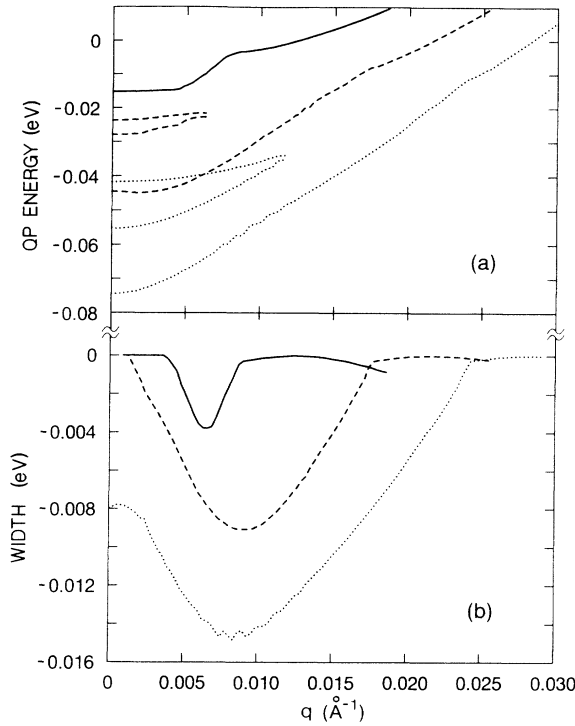


FIG. 3. Quasiparticle energy (a) and width (b) dispersion for a 2D electron gas at $T=0$ K. Solid line: $n_S=2.2 \times 10^{11} \text{ cm}^{-2}$; dashed line: $n_S=7.1 \times 10^{11} \text{ cm}^{-2}$; dotted line: $n_S=1.2 \times 10^{12} \text{ cm}^{-2}$.

is on the same curve as the solution that gives the δ function at $k=k_F$. In 3D, the plasmaron band is separated from the band that gives the δ function at $k=k_F$.¹

This difference between the 2D and the 3D case also appears in the DOS. Figure 4 displays the DOS for three values of the chemical potential ($\mu=2.7, 13.7, \text{ and } 27.4$ meV). The corresponding densities are $n_S=2.2 \times 10^{11} \text{ cm}^{-2}$, $n_S=7.1 \times 10^{11} \text{ cm}^{-2}$, and $n_S=1.25 \times 10^{12} \text{ cm}^{-2}$. Whereas in 3D the plasmaron produces a satellite peak below the edge of the noninteracting electron DOS,¹ in 2D it produces a staircaselike structure with three steps.

The first two steps are associated with the two peaks in the spectral function at $k=0$. The first step is a discontinuity at low density because the plasmaron peak is a δ function. The third step is associated with the beginning of the region where the quasiparticle damping is small and where the curvature of the energy dispersion decreases (see Fig. 3). The height of the third step is proportional to the variation of the curvature and is larger at low density. The peaks at the edge of the steps in the DOS are explained by the dispersion of the quasiparticle energy. The enhancement at the edge of the first step is due to terms of k of an order higher than quadratic. It is stronger at low-density. The peak at the edge of the third step is associated with a flat portion in the quasiparticle energy dispersion at $k \neq 0$.

It is interesting to note that whereas in 3D the structures in the DOS related to the plasmaron are stronger at high density, in 2D the steps in the DOS are sharper at low density.

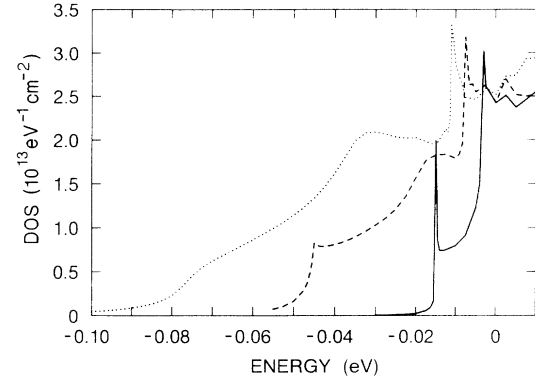


FIG. 4. Density of states for a 2D electron gas at $T=0$ K. Solid line: $n_S=2.2 \times 10^{11} \text{ cm}^{-2}$; dashed line: $n_S=7.1 \times 10^{11} \text{ cm}^{-2}$; dotted line: $n_S=1.2 \times 10^{12} \text{ cm}^{-2}$.

IV. BAND RENORMALIZATION

Figure 5 displays the shift of the chemical potential $\Delta^{(\mu)}$ and of the edge of the DOS, $\Delta^{(\text{DOS})}$, computed as described in Sec. II. We see that $\Delta^{(\mu)}$ is smaller than $\Delta^{(\text{DOS})}$. The difference between $\Delta^{(\mu)}$ and $\Delta^{(\text{DOS})}$ is due to the fact that the DOS is quite different in an interacting and in a noninteracting electron gas (see Fig. 4). This difference can be ascribed to the shape of the quasiparticle energy dispersion that is not parabolic and also to the contribution of the imaginary part of the self-energy.

Figure 4 shows that with increasing density the shape of the DOS becomes more different from that for a noninteracting electron gas. In particular, the tail extends to lower energy. This explains why the difference between $\Delta^{(\mu)}$ and $\Delta^{(\text{DOS})}$ increases with increasing density.

At this point I would like to emphasize that Luttinger's theorem cited in Sec. II is entirely fulfilled when the charge density is given by (4). The Fermi momentum is determined here by the intersection of the quasiparticle energy dispersion with the $E=0$ axis (see Fig. 3). This provides us with a good indication for the numerical accuracy of the evaluation of the band renormalization.

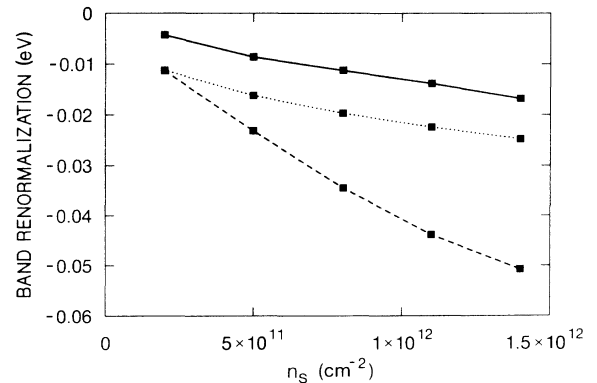


FIG. 5. Band renormalization for a 2D electron gas at $T=0$ K. Solid line: shift of the chemical potential (full RPA); dashed line: shift of the edge of the DOS (full RPA); dotted line: lowest-order approximation.

Figure 5 also displays the shift of the chemical potential $\Delta^{(0)}$ computed by using the approximation described in Sec. II [see (6)]. This curve lies between the curves for $\Delta^{(\mu)}$ and $\Delta^{(\text{DOS})}$. Its variation with the density is parallel to that of $\Delta^{(\mu)}$. It is interesting to note that at $k = k_F$, $E = 0$ is the solution of (5) and hence that the chemical potential with the density computed with (4) is given by

$$\mu = \mu^{(0)} + S_R(k_F, 0). \quad (8)$$

The difference from (6) is that in (8) the self-energy is calculated using the chemical potential of the interacting electron gas μ . Hence, the difference between $\Delta^{(\mu)}$ and $\Delta^{(0)}$ is due to the lowest-order approximation made in (6).

In the literature, the DOS is often assumed to have the same shape in the interacting and in the noninteracting electron gas. Its edge is assumed to shift to lower energy in the interacting electron gas by the same amount $\Delta^{(0)}$ as the chemical potential does (rigid shift approximation). Figure 5 clearly shows that this is not a very good approximation since $\Delta^{(\mu)}$ and $\Delta^{(\text{DOS})}$ are quite different. For the comparison with experimental data $\Delta^{(\mu)}$ or $\Delta^{(\text{DOS})}$ should be used, depending on the measurement to be interpreted. For example, $\Delta^{(\text{DOS})}$ should be used when studying optical data such as photoluminescence spectra, and $\Delta^{(\mu)}$ should be used when studying transport measurements.

The renormalized effective mass m^* is usually defined at $k = k_F$ by the following equation:¹⁶

$$\frac{\hbar^2 k_F}{m^*} = \left. \frac{dE^{(\text{QP})}}{dk} \right|_{k=k_F}. \quad (9)$$

In this definition, the quasiparticle energy dispersion is assumed to be parabolic with an effective mass m^* . Figure 3 shows that this is not the case if $E^{(\text{QP})}$ is the solution of (5), especially at low density. The quasiparticle energy dispersion has two sections. The low-momentum section starts with a flat region followed by a high curvature region. The high-momentum section is parabolic with a lower curvature. We then see that, through (9), the effective mass is determined by the curvature of the high-momentum section. Figure 6 displays the variation with the density of the relative mass renormalization.

In the lowest-order approximation, the quasiparticle

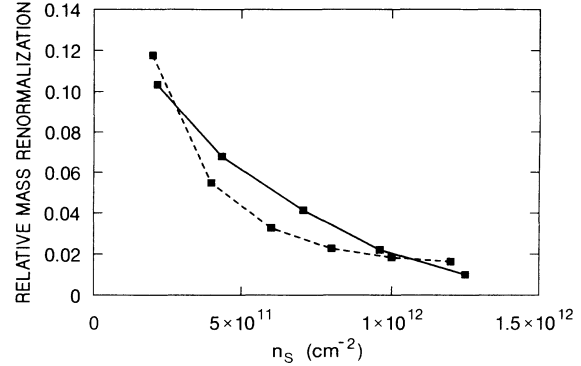


FIG. 6. Relative mass renormalization $(m^* - m)/m$ at the Fermi surface for a 2D electron gas at $T = 0$ K. Solid line: full RPA; dashed line: lowest-order approximation.

energy is given by

$$E^{(\text{QP})}(k) = \xi(k) + S_R^{(0)} \left[k, \frac{\hbar^2(k^2 - k_F^2)}{2m} \right]. \quad (10)$$

In the literature, this expression is often used in conjunction with (9) to evaluate the effective-mass renormalization.⁸ Figure 6 displays the corresponding variation with density of the relative mass renormalization. I feel that the difference with the other, more exact, procedure is small if compared with the fluctuations of the experimental data available in the literature.

V. CONCLUSION

It has been shown that the difference in the plasmon energy dispersion is responsible for the difference between 2D and 3D plasmaron excitation. This work also shows that the renormalization of the chemical potential is not equal to that of the edge of the DOS and hence that the rigid shift approximation should be abandoned. Finally, it is shown that the renormalization of the effective mass is almost the same whether evaluated using the exact or the lowest-order approximation quasiparticle energy dispersion.

ACKNOWLEDGMENT

I am grateful to A. Baratoff for many fruitful discussions.

*Present address: Beckman Institute, University of Illinois at Urbana-Champaign, Urbana, IL 61801; Electronic address: vonallmen@gate.spg.uiuc.edu

¹B. I. Lundquist, Phys. Kondens. Mater. **6**, 193 (1967); **6**, 206 (1967); **7**, 117 (1968).

²L. Hedin and S. Lundqvist, *Solid State Physics, Advances in Research and Applications* (Academic, New York, 1969), Vol. 23.

³B. Vinter, Phys. Rev. Lett. **35**, 1044 (1975); Phys. Rev. B **13**, 4447 (1976); **15**, 3947 (1977).

⁴R. K. Kalia, S. Das Sarma, M. Nakayama, and J. J. Quinn, Phys. Rev. B **18**, 5564 (1978).

⁵G. E. W. Bauer and T. Ando, J. Phys. C **19**, 1537 (1986).

⁶C. S. Ting, T. K. Lee, and J. J. Quinn, Phys. Rev. Lett. **34**, 870 (1975).

⁷S. Das Sarma, R. Jalabert, and S.-R. E. Yang, Phys. Rev. B **41**, 8288 (1990).

⁸S. Yarlagadda and G. F. Giuliani, Phys. Rev. B **38**, 10966 (1988).

⁹G. Bongiovanni, J.-L. Staehli, and C. Bosio, Superlatt. Micro-

- struct. **8**, 81 (1990).
- ¹⁰S. Das Sarma and B. Vinter, Phys. Rev. B **26**, 960 (1982), and references therein.
- ¹¹See, e.g., G. D. Mahan, *Many-Particle Physics* (Plenum, New York, 1986).
- ¹²F. Stern, Phys. Rev. Lett. **18**, 546 (1967).
- ¹³J. M. Luttinger, Phys. Rev. **119**, 1153 (1960).
- ¹⁴L. Hedin, Phys. Rev. **139**, A796 (1965).
- ¹⁵G. D. Mahan and C. B. Duke, Phys. Rev. **149**, 705 (1966).
- ¹⁶See, e.g., E. M. Lifshitz and L. P. Pitaevskii, *Statistical Physics, Part 2* (Pergamon, Oxford, 1986).

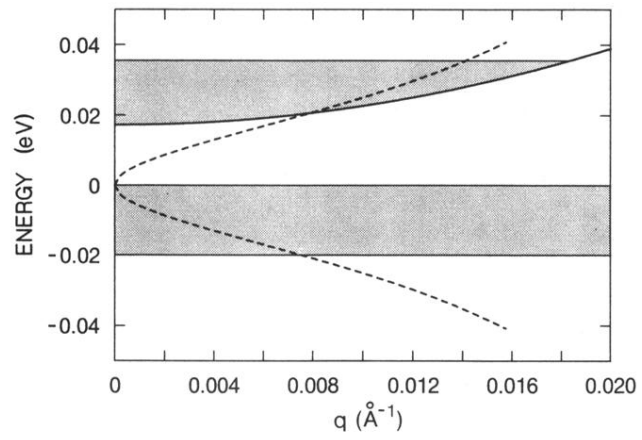


FIG. 2. Electron (solid line) and plasmon (dashed line) energy dispersion for a 2D electron gas. The initial energy in the electron-plasmon scattering ω is subtracted from the electron energy. The shaded areas indicate the regions where the scattered state is allowed to be at $T=0$ K.